The Role of Micelle Size in Tumor Accumulation, Penetration, and Treatment

Jinqiang Wang,[†] Weiwei Mao,[†] Lye Lin Lock,[§] Jianbin Tang,[*,†] Meihua Sui,[†,#] Weilin Sun,[‡] Honggang Cui,[§] Dong Xu,[⊥] and Youqing Shen[†]

[†]State Key Laboratory of Chemical Engineering and Center for Bionanoengineering, College of Chemical and Biological Engineering, Zhejiang University, Hangzhou 310027, China, [‡]Department of Polymer Science and Engineering, Zhejiang University, Hangzhou 310027, China, [§]Department of Chemical and Biomolecular Engineering, Johns Hopkins University, Baltimore, Maryland 21218, United States, and [⊥]The Second Affiliated Hospital, Zhejiang University School of Medicine, Hangzhou 310027, China. [#]Present address: [#]Zhejiang Provincial People's Hospital, Hangzhou, China.

ABSTRACT The specific sizes that determine optimal nanoparticle tumor accumulation, penetration, and treatment remain inconclusive because many studies compared nanoparticles with multiple physicochemical variables (*e.g.*, chemical structures, shapes, and other physical properties) in addition to the size. In this study, we synthesized amphiphilic block copolymers of 7-ethyl-10-hydroxylcamptothecin (SN38) prodrug and fabricated micelles with sizes ranging from 20 to 300 nm from a single copolymer. The as-prepared micelles had exactly the same chemical structures and similar physical properties except for size, which provided an ideal platform for a systematic investigation of the size effects in cancer drug delivery. We found that the micelle's blood circulation time and tumor accumulation increased with the increase in their diameters, with optimal diameter range of 100 to 160 nm. However, the much higher tumor accumulation of the large micelles (100 nm) did not result in significantly improved therapeutic efficacy, because the large micelles had poorer tumor penetration than the small ones (30 nm). An optimal size that balances drug accumulation and penetration in tumors is critical for improving the therapeutic efficacy of nanoparticulate drugs.

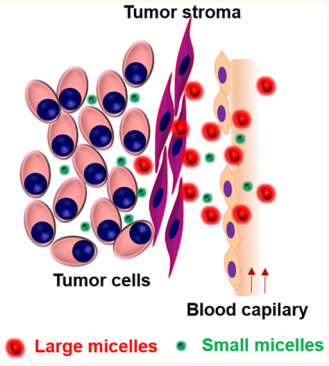

KEYWORDS: cancer drug delivery · 7-ethyl-10-hydroxylcamptothecin · polymeric micelle · size effect · tumor penetration

Nanoparticulate drugs that consist of drugs and nanocarriers, such as lipids and polymers, have great potential in cancer chemotherapy because of their improved pharmacokinetics and cellular uptake.[1−6] They can preferentially accumulate in tumors through the enhanced permeability and retention effect resulting from the abnormal porous blood capillaries and deficient lymphatic drainage of tumors. Thus, nanoparticulate drugs may significantly reduce side effects and improve therapeutic efficacy.[7−9] To date, a number of nanoparticulate drugs based on liposomes or polymers have entered into clinical trials for cancer therapy; Doxil, DaunoXome, Abraxane, and Genexol-PM have already been approved for clinical use.[8] Although clinical studies have indicated that these drugs could reduce the side effects, they barely showed superiority over the free drugs in terms of overall survival of patients.[9,10] A systematic study of the delivery process and a rational design of nanoparticulate drugs are needed to develop next-generation delivery systems.

A nanoparticulate drug for systemic treatment of solid tumors should generally undergo a five-step [*i.e.*, circulation, accumulation, penetration, internalization, and release (*CAPIR*)] cascade to transport drugs into cancer cells to exert their therapeutic action.[11−14] The overall efficiency in completing the *CAPIR* cascade is determined by the physical and chemical characteristics of nanoparticles,[15,16] including stability,[17] surface properties (*e.g.*, PEG chain length and density,[18] targeting groups,[12] as well as surface charges[19]), size,[18] and shape.[20,21] Among these factors, the size of nanoparticles affects the entire cascade and plays a critical role in drug delivery. The size effects have been extensively studied, but the findings were rather controversial. Perrault *et al.* found that PEGylated gold nanoparticles with size of 60 nm had the highest tumor

* Address correspondence to jianbin@zju.edu.cn.

Received for review April 3, 2015 and accepted July 6, 2015.

Published online July 06, 2015
10.1021/acsnano.5b02017

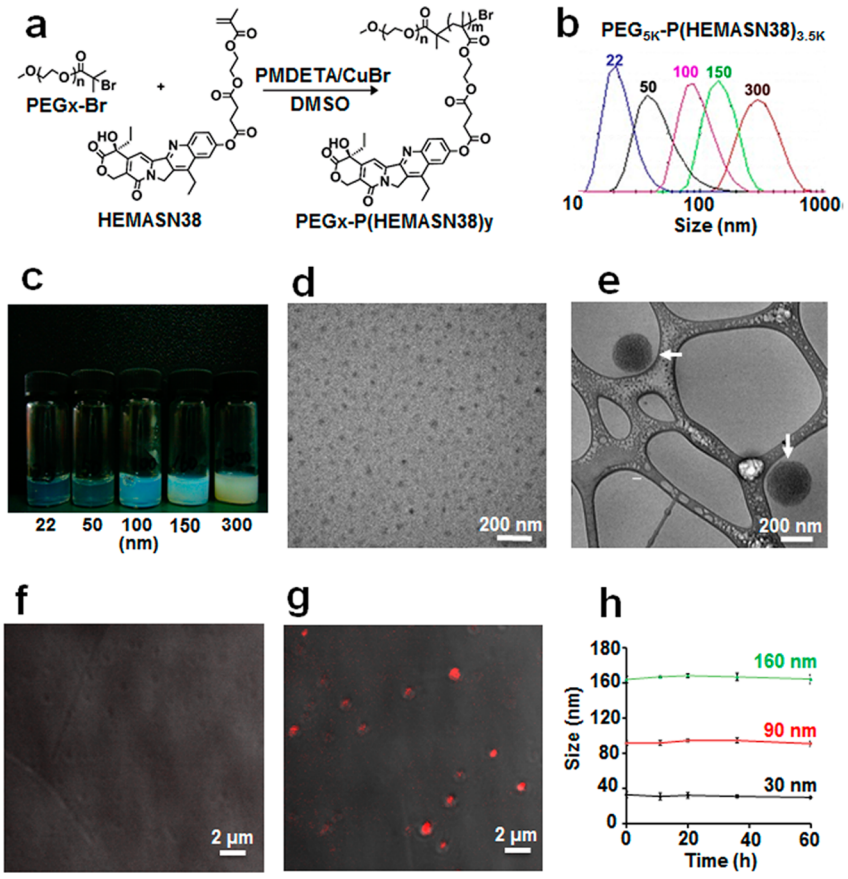

Figure 1. Synthesis of PEG_x-P(HEMASN38)$_y$ and characterizations of their micelles. (a) Synthesis of PEG_x-P(HEMASN38)$_y$ *via* ATRP. (b) Size distributions of the micelles prepared from PEG_{5K}-P(HEMASN38)$_{3.5K}$ with different methods measured by DLS at SN38-eq concentration of 1 mg/mL. (c) Images of the micelle solutions with sizes ranging from 22 to 300 nm. (d) Representative TEM image of the 22 nm micelles. Scale bar, 200 nm. (e) Representative cryo-TEM image of the 180 nm micelles. Scale bar, 200 nm. (f, g) Fluorescent images of the (f) 100 and (g) 170 nm micelles prepared in the presence of rhodamine B (0.1 mg/mL). Scale bar, 1 μm. (h) Changes in the size of different micelles incubated in 100% fetal bovine serum (FBS) at 37 °C over time.

accumulation among 20, 40, 60, 80, and 100 nm nanoparticles,[18] whereas Huang *et al.* found that ultrasmall (*e.g.*, 2 and 6 nm) gold nanoparticles coated with tiopronin had longer blood circulation time than 15 nm gold nanoparticles.[22] Lee *et al.* showed that 25 nm micelles were cleared more rapidly from the blood circulation than the 60 nm micelles, which led to an approximately 2-fold decrease in total tumor accumulation.[23] However, Cabral *et al.* found that sizes from 30 to 100 nm did not affect the blood clearance, tumor accumulation, and anticancer activity of micelles in hyperpermeable tumors.[24] The conflicting observations in size effects were ascribed to the different chemical structures and physical properties of the nanoparticles used for the size effect studies. For instance, different sized polymeric micelles were usually fabricated from different copolymers with varied block lengths or ratios.[25,26] These micelles differed not only in sizes but also in other chemical and physical properties, such as micelle stability, surface charge, softness, PEG chain length, hydrophilic shell thickness, and chain density. Therefore, the size effects of micelles on their *CAPIR* cascade and anticancer activity have not been successfully elucidated.

In this study, we synthesized amphiphilic block copolymers PEG_x-P(HEMASN38)$_y$ from a prodrug monomer of a potent anticancer drug 7-ethyl-10-hydroxylcamptothecin (SN38) with controlled block lengths. By manipulating the preparation methods, we managed to fabricate stable micelles of varying sizes ranging from 20 to 300 nm from a single block copolymer. These polymeric prodrug micelles had identical chemical structures but different sizes, which enabled us to conduct a systematic study on the effects of particle size on the *CAPIR* capability and anticancer activity of polymeric micelles without influence from other factors.

RESULTS

Synthesis of Prodrug Copolymers and Fabrication of Micelles. The prodrug monomer, 10-OH methacrylate ester of SN38 (HEMASN38), and its atom transfer radical polymerization (ATRP) with polyethylene glycolyl monomethyl ether 2-bromoisobutyrate (PEG-Br) as macroinitiator are shown in Figure 1a. Through the use of PEG-Br

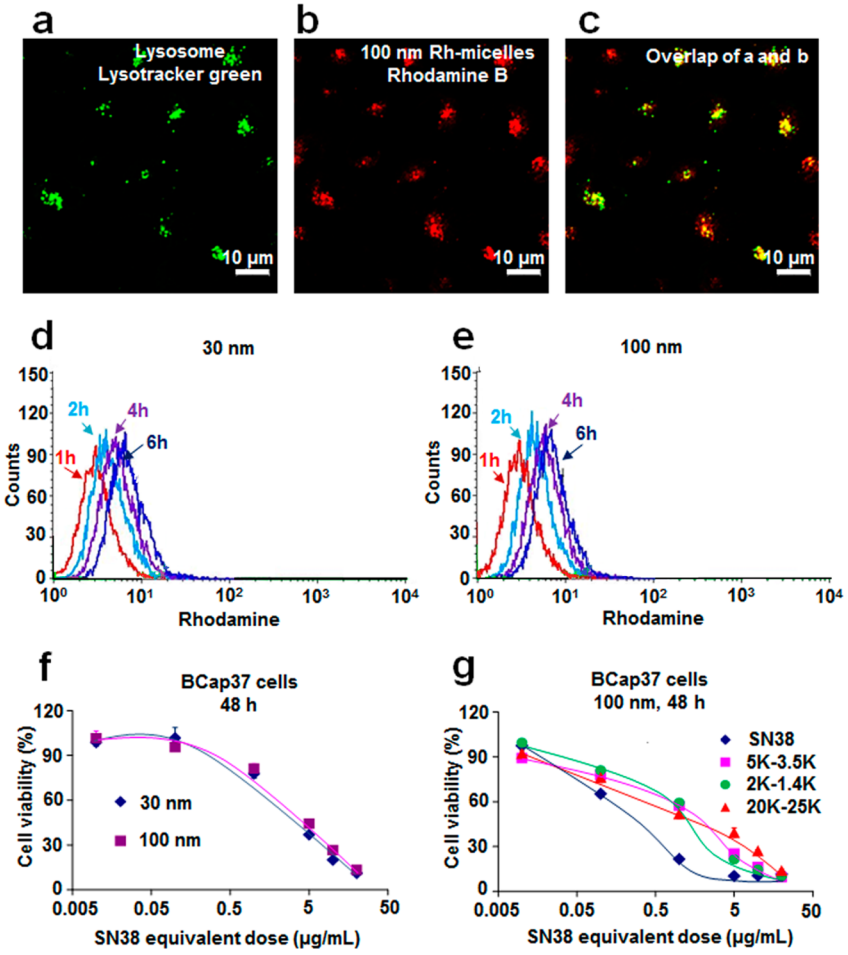

Figure 2. Intracellular distribution (a–c), cellular uptake (d, e), and the cytotoxicities (f, g) of the micelles. (a–c) CLSM images of BCap37 cells cultured with 100 nm PEG_{5K}-$P(HEMASN38)_{3.5K}$ rhodamine B-labeled micelles (Rh-micelles; at SN38-eq dose of 5 μg/mL) for 1.5 h and then LysoTracker green (200 nM, 1.5 h). Images were taken from the LysoTracker green channel (green, a), the rhodamine B channel (red, b), and their overlapped channel (c). (d, e) BCap37 cells were cultured with (d) 30 and (e) 100 nm Rh-micelles from PEG_{5K}-$P(HEMASN38)_{3.5K}$ (at SN38-eq dose of 10 μg/mL) for different times, and the fluorescence intensities at 575 nm–620 nm (excited at 488 nm) were measured by flow cytometry. (f, g) Representative dose-dependent cytotoxicities to BCap37 cells of the micelles with different sizes made from (f) PEG_{5K}-$P(HEMASN38)_{3.5K}$ or (g) with the same 100 nm size from different block copolymers.

of different molecular weights (2, 5, and 20 kDa) and by changing the monomer-to-initiator (HEMASN38/PEG-Br) molar ratio, we prepared a series of prodrug copolymers with different block lengths, namely, PEG_{2K}-$P(HEMASN38)_{1.4K}$, PEG_{5K}-$P(HEMASN38)_{3.5K}$, PEG_{5K}-$P(HEMASN38)_{7K}$, and PEG_{20K}-$P(HEMASN38)_{25K}$, as determined from their NMR spectra. The block copolymers had polydispersity indices close to those of the macroinitiators (M_w/M_n = 1.2), which suggested that the resulting poly(HEMASN38) block lengths were also uniform.

The polymeric micelles were prepared from the amphiphilic block copolymers *via* the dialysis method.[27] Notably, we found that one amphiphilic PEG_x-$P(HEMASN38)_y$ could form micelles of distinct sizes by varying the water-miscible organic solvent, the block copolymer concentration, and even the mixing sequence. For example, the direct dropwise addition of a solution (5 mg/mL) of PEG_{5K}-$P(HEMASN38)_{3.5K}$ in DMF to deionized water produced 22 nm micelles, as measured by dynamic light scattering (DLS), but 50 nm micelles were produced when a solution (2.5 mg/mL) of PEG_{5K}-$P(HEMASN38)_{3.5K}$ in DMSO was used instead. Alternatively, adding water to the PEG_{5K}-$P(HEMASN38)_{3.5K}$/DMSO solution (3 mg/mL) produced 100 nm micelles. In addition, increasing the copolymer concentration produced larger micelles (*e.g.*, 150 and 300 nm micelles). The produced micelles with sizes ranging from 22 to 300 nm are shown in Figure 1b, c. The micelles of different sizes from the other three copolymers were prepared similarly (Figure S1).

The micelles exhibited low polydispersity with PDI of less than 0.2. Very interestingly, they were all spherical nanoparticles independent of sizes, as observed by TEM and cryo-TEM (Figures 1d, 1e, and S2). The ability of the micelles to load water-soluble fluorescent dye was also used to probe their structures (*e.g.*, solid-core micelles or vesicles).[29] All micelles

(⩽ 100 nm) could not load water-soluble dyes, such as rhodamine B, which indicated that they were typical core−shell micelles with hydrophobic cores (Figures 1f and S3). However, the larger micelles, *i.e.*, 150 or 300 nm, could load rhodamine B, as observed by confocal laser scanning microscopy (CLSM) (Figures 1g, S4, and S5), which suggested that these micelles were vesicles or compound micelles with aqueous interiors. Noteworthy, all micelles from the same copolymer had identical chemical structures, but different PEG chain densities. For the core−shell micelles, the PEG chain density increased with the increase of the size of micelles.[26]

The micelles were all very stable in PBS 7.4 and even in the presence of FBS as observed by DLS (Figures 1h and S6). All micelles, regardless of size, had zeta potentials of approximately −4 mV. Additionally, the micelles had similar burst-free slow release of SN38, which was less than 20% in PBS 7.4 in 80 h, independent of the block copolymer types and sizes, and the SN38 release rate was accelerated in the presence of GSH (Figure S7). *In vitro* cellular uptake experiments showed that the PEG_{5K}-$P(HEMASN38)_{3.5K}$ micelles were internalized *via* endocytosis and mainly localized in lysosomes (Figure 2a−c). The rate of endocytosis was also size-independent as measured by flow cytometry (Figure 2d, e). Accordingly, 30 and 100 nm micelles showed similar cytotoxicities (Figure 2f). Furthermore, the micelles randomly selected from other PEG_x-$P(HEMASN38)_y$ also exhibited similar cytotoxicities (Figure 2g).

Blood Circulation and Biodistribution. The blood clearance of an array of 18 micelles from PEG_x-$P(HEMASN38)_y$ after single intravenous injection was examined using ICR mice (Figure 3). To compare different micelles, the equivalent dose in terms of nanoparticle surface area may be used,[18] but the equivalent dose in terms of mass is more clinically relevant and thus was used in the current study. The blood clearance of PEG_{2K}-$P(HEMASN38)_{1.4K}$ micelles became slower as the size increased from 30 to 160 nm (Figure 3a). The 30 nm micelles were quickly cleared from the bloodstream, but the blood clearance of 160 nm particles was very slow. The micelles made from PEG_{5K}-$P(HEMASN38)_{3.5K}$ with doubled block lengths had a similar size-dependent trend, but their clearance rates were much slower than those made from PEG_{2K}-$P(HEMASN38)_{1.4K}$ with similar sizes (Figure 3b). Among these micelles, the 100 and 150 nm micelles had ultraslow clearance rates, contrary to the 300 nm ones, which were cleared quickly. Very similar ultraslow clearances were found in the micelles with similar sizes (110 and 160 nm) from PEG_{5K}-$P(HEMASN38)_{7K}$ with the same PEG but longer poly(HEMASN38) block. The small (30 and 70 nm) PEG_{5K}-$P(HEMASN38)_{7K}$ micelles were cleared faster than the PEG_{5K}-$P(HEMASN38)_{3.5K}$ micelles of the same size (Figure 3b and 3c). Very interestingly, the clearance of the micelles made from PEG_{20K}-$P(HEMASN38)_{25K}$ with two long blocks was less sensitive to size (Figure 3d). Further analysis of the blood clearance profiles of all micelles showed a clear difference at about 100 nm. Micelles (<100 nm) were cleared quickly and even faster as the size became smaller, while those approximately 100 to 160 nm were cleared very slowly. Even after 20 h, the blood concentrations of the latter were still higher than 10% of the initial concentration.

The calculated blood circulation half-life times ($t_{0.5\beta}$) and area-under-curve (AUC) values of the micelles are listed in Table 1. Both the PEG chain length and the mass fraction of PEG in the block copolymer affected the pharmacokinetics of the micelles.[26] It needs to be noted that, for solid-core micelles (<100 nm) prepared from same PEGx-P(HEMASN38)y, the increase in the micelle size also increased the density of PEG chain on the surface of micelles.[26] Thus, we herein defined the product of PEG molecular weight (M_{PEG}) in kDa and its mass fraction in the block copolymer, as a PEGylation factor for simplification. The $t_{0.5\beta}$ and AUC as functions of micelle size and PEGylation factor are plotted and shown in Figure 4a and 4b. Clearly, both the PEGylation factor and size affected their $t_{0.5\beta}$ and AUC, but the size played a more determinant role. When the PEGylation factor was higher than 2.5, the $t_{0.5\beta}$ and AUC values increased only slightly as the PEGylation factor increased. Both $t_{0.5\beta}$ and AUC values were low for micelles <100 nm and peaked in the size range from 100 to 160 nm. For PEG_{5K}-$P(HEMASN38)_{3.5K}$, the $t_{0.5\beta}$ was as short as 1 and 5.9 h for the 22 and 50 nm micelles, respectively, but increased to 7.2 and 12.7 h for the 100 and 150 nm micelles, respectively. However, the $t_{0.5\beta}$ of the further larger micelles, namely, the 300 nm particles, sharply decreased to 3.3 h, and its AUC was reduced to 104%·h, which was approximately 1/8 of that for the 150 nm micelle.

The biodistributions of the micelles in the main organs were evaluated. PEG_{5K}-$P(HEMASN38)_{3.5K}$ micelles with sizes of 35, 100, and 150 nm were selected to determine the size effects on the biodistribution. As shown in Figure 4c and S8, the MPS organs, the liver and spleen sequestered most micelles, and they had different preferences in the uptake of micelles with varying sizes (Figures S9 and S10). Consistent with the fast blood clearance, the 35 nm micelles quickly accumulated in the liver with the highest drug concentration of 84% ID/g (percentage of injected dose per gram tissue) at 6 h postinjection, and a decayed one of 45% ID/g at 24 h postinjection (Figures 4c, S8a, and S9). The liver accumulation of the 100 nm micelles slightly increased over time but was much lower than that of the 35 nm micelles. The drug concentrations of the former in the liver were only 12.7% and 20% ID/g at 6 and 24 h postinjection, respectively (Figures 4c and S8b). Contrary to the 35 and 100 nm micelles, the 150 nm micelles had much higher accumulation in the

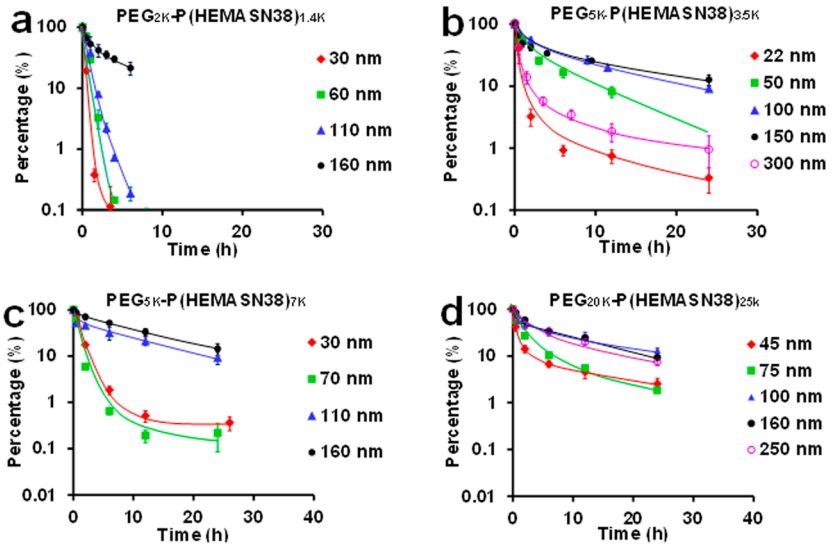

Figure 3. Normalized blood clearance profiles in terms of the percentage of the injected dose as a function of time after intravenous administration of micelles. ICR mice were injected with micelle PBS solutions at an SN38-eq dose of 5 mg/kg *via* the tail vein. The SN38 concentration in the blood was determined by HPLC. The SN38 blood concentration at 2 min was set to 100%. Data are means ± SD (n = 3).

TABLE 1. Blood Half-Life and Area under Curve for Different Micelles of ICR Mice and Nude Mice Treated at an SN38-eq Dose of 5 mg/kg[a]

PEG_{5k}-$P(SN38)_{3.5k}$	size (nm)	22 (30)	50	100 (110)	150 (160)	300
	$t_{0.5\beta}$ (h)	1.0 (1.9)	5.9	7.2 (17.7)	12.7 (20.0)	3.3
	AUC (%·h)	77 (124)	345	700 (1295)	830 (1142)	104
PEG_{5k}-$P(SN38)_{7k}$	size (nm)	30	70	110	160	—
	$t_{0.5\beta}$ (h)	1	0.6	9.4	9.5	—
	AUC (%·h)	131	88	716	1115	—
PEG_{2k}-$P(SN38)_{1.4k}$	size (nm)	30	60	110	160	—
	$t_{0.5\beta}$ (h)	0.2	0.6	0.7	4.2	—
	AUC (%·h)	31	92	102	368	—
PEG_{20k}-$P(SN38)_{25k}$	size (nm)	45	75	100	160	250
	$t_{0.5\beta}$ (h)	6.3	3.7	13.7	10.4	8.6
	AUC (%·h)	181	229	942	837	680

[a] The data in brackets was obtained on nude mice.

spleen than in the liver, and the splenic accumulation increased over time, which reached 192% ID/g at 24 h postinjection (Figures 4c, S8c). Similarly, the liver accumulation of the 150 nm micelles also increased over time and reached 51% ID/g at 24 h postinjection, which was higher than that of 100 nm micelles at the same time point.

Given that a size of around 100 nm is apparently a critical size between slow and fast blood clearance for the micelles, we compared the biodistributions of the micelles from different copolymers with similar sizes of approximately 100 nm (Figure S8d–f). The micelles from PEG_{5K}-$P(HEMASN38)_{7K}$ and PEG_{20K}-$P(HEMASN38)_{25K}$ exhibited similar biodistributions to those of the PEG_{5K}-$P(HEMASN38)_{3.5K}$ micelles, which showed low accumulation in the liver and spleen. However, the micelles from PEG_{2K}-$P(HEMASN38)_{1.4K}$ were sequestered quickly from the blood into the liver and the spleen (Figure 4c).

Tumor Accumulation. The size effect on the tumor accumulation after intravenous injection was first probed with 35, 100, and 150 nm PEG_{5K}-$P(HEMASN38)_{3.5K}$ micelles using nude mice bearing BCap37 xenografted tumors (Figure 5a). The drug concentration in the tumor of 35 nm micelles was 3.5% ID/g both at 0.5 and 6 h, and decreased to 1.5% ID/g at 24 h postinjection. The tumor accumulations of both 100 and 150 nm micelles increased over time and reached 12% and 14.6% ID/g at 24 h post injection, respectively, almost 10 times that for the 35 nm micelles.

The effect of the copolymer structure on the tumor accumulation was investigated using the micelles with similar sizes of around 100 nm but made from four different copolymers (Figure 5b). The tumor drug concentrations of the micelles from PEG_{5K}-$P(HEMASN38)_{7K}$ and PEG_{20K}-$P(HEMASN38)_{25K}$ also increased over time and reached 12% and 21% ID/g at 24 h postinjection, respectively. However, the micelles from PEG_{2K}-$P(HEMASN38)_{1.4K}$ had much lower tumor accumulation, and its tumor drug concentration decreased from 2.6% ID/g at 2 h to 1.5% ID/g at 10 h postinjection.

Tumor Penetration. The tumor penetration ability of the micelles was observed using Rh-micelles on Bcap37 xenografted tumors (Figure 5c–k). The mice bearing xenografted Bcap37 tumors were first intravenously injected with the micelles. Then, 5 min prior to the sacrifice of the mice, FITC-labeled *Lycopersicon esculentum* lectin (1 mg/kg) was intravenously injected to mark tumor blood vessels (green) for observation using CLSM. The red fluorescence in the tumor treated with 100 nm micelles (red spots) was much stronger than that in the tumor treated with the 30 nm micelles at 24 h postinjection. This finding was consistent to the early observed size-dependent tumor accumulation.

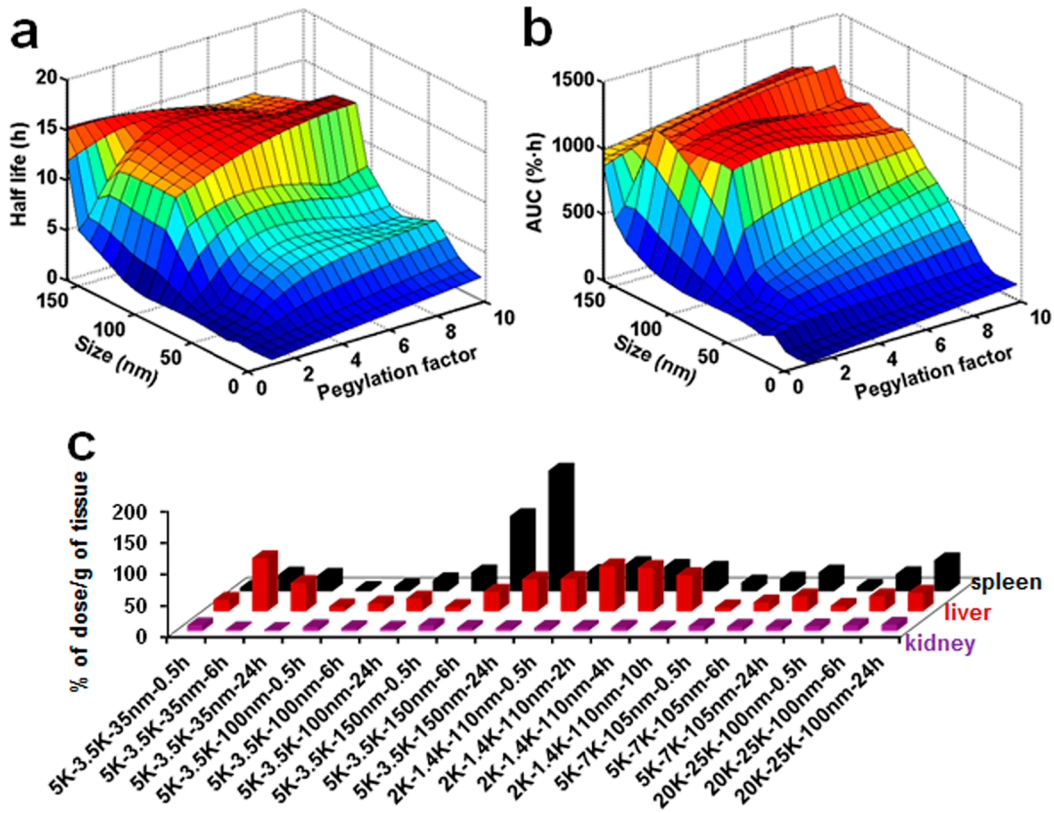

Figure 4. Blood compartment pharmacokinetics and biodistribution of micelles. (a, b) The calculated (a) half-life times ($t_{0.5\beta}$) and (b) areas under curve (AUC) of the micelles as functions of their sizes and PEGylation factors. These two figures were plotted using software Matlab. (c) The time-dependent biodistribution for micelles of different sizes or 100 nm micelles from different copolymers in the three main organs. Nude mice bearing tumors of *ca.* 100 mm^3 were intravenously injected with micelles at an SN38-eq dose of 5 mg/kg. At timed intervals, the mice (n = 3) were sacrificed, and the SN38 concentration in the organs were determined by HPLC. The $t_{0.5\beta}$ and AUC were estimated by fitting the SN38 concentration in plasma into a two compartment model (Loo−Riegelman method) by the nonlinear least-squares method using 3P87 software.

However, the red fluorescence in the tumor treated with 100 nm micelles was mostly associated with the green blood capillary and aggregated into large particles, whereas the red fluorescence in the tumor treated with 30 nm micelles was observed in the regions away from the green blood vessels (Figure 5c, d). Multifunctional cytokine transforming growth factor TGF-β regulates the progression of cancer through affecting tumor microenvironment and cancer cells. Inhibition of TGF-β signaling was reported able to improve the penetration of nanoparticles in poorly permeable tumors.[28] The TGF-β inhibitor (TGF-β-I, LY364947) was administrated *via* intraperitoneal injection with a dose of 1 mg/kg at 1 h before 100 nm Rh-micelles were i.v. injected. The red fluorescence in the tumor treated with 100 nm micelles plus TGF-β-I distributed broader and showed stronger fluorescence in the region away from blood vessels than that treated only with 100 nm micelles (Figure 5e), indicating TGF-β-I could increase the penetration of 100 nm micelles in tumor. To quantitatively compare the penetration of 30 nm micelles, 100 nm micelles with and without TGF-β-I, the red fluorescence intensities as a function of distance from blood vessels (0−100 μm) in a representative region were measured. The 30 nm micelles had weaker red fluorescence, but they penetrated farther away the blood vessels. By contrast, the 100 nm micelles had much stronger red fluorescence, but had shorter penetration in tumor, which could be improved by treatment with TGF-β-I (Figure 5f−h).

To more fairly compare the penetration capability of the two micelles in the tumor, PEG_{5K}-$P(HEMASN38)_{3.5K}$ was separately conjugated with FITC or rhodamine B and used to fabricate different sized micelles labeled with different fluorescence dyes (30 nm FITC-labeled micelles *vs* 100 nm Rh-micelles). The two micelle solutions at equal fluorescence intensities were mixed, and 10 μL of this solution was intratumorally injected. After 72 h, the tumors were excised and observed by CLSM (Figure 5i−k). Clearly, the 30 nm green FITC-labeled micelles diffused much further away from the injection site compared with the 100 nm red Rh-micelles, which stayed around the injection site.

***In Vivo* Anticancer Activity.** The *in vivo* antitumor activities of the two different sized micelles from both PEG_{5K}-$P(HEMASN38)_{3.5K}$ (30 nm *vs* 100 nm) and PEG_{20K}-$P(HEMASN38)_{25K}$ (50 nm *vs* 100 nm) were subsequently evaluated using nude mice bearing BCap37

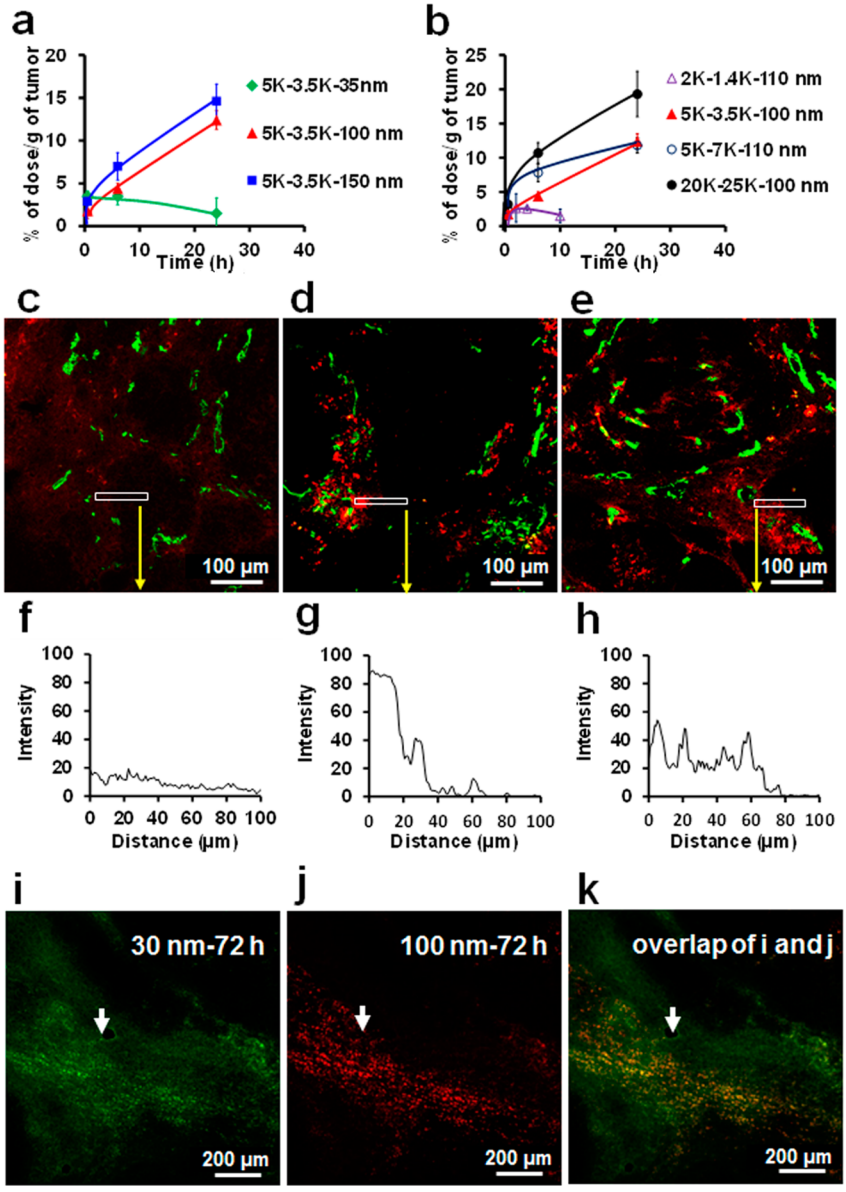

Figure 5. Tumor accumulation of intravenously injected micelles and the intratumoral distribution of micelles with different sizes after intravenous administration or intratumoral injection. (a, b) The tumor accumulation of the micelles with different sizes from PEG_{5K}-$P(HEMASN38)_{3.5K}$ (a) or 100 nm micelles from different copolymers (b). (c–e) Nude mice bearing BCap37 xenografted tumors of *ca*. 100 mm^3 were directly intravenously injected with 30 nm (c) or 100 nm Rh-micelles (d) from PEG_{5K}-$P(HEMASN38)_{3.5K}$ at an SN38-eq dose of 5 mg/kg or the mice was first intraperitoneally treated with TGF-β inhibitor (LY364947) at a dose of 1 mg/kg 1 h before intravenously injection of 100 nm Rh-micelles (e). Immediately before termination at 24 h postinjection of the micelles, the mice were injected with FITC-labeled *Lycopersicon esculentum* lectin to label blood vessels (green). The tumors were excised and sectioned into 10 μm thick slices and observed by CLSM. The micelles are shown in red. (f–h) The red fluorescence intensity profile as a function of distance from blood vessels (0–100 μm) in a representative region (indicated by the white rectangle) was plotted by *software ImageJ*. (i–k) The FITC labeled 30 nm micelles and 100 nm Rh-micelles were mixed at equal fluorescence intensities. This mixture (10 μL) was injected into a tumor. The tumor was excised after 72 h, and its slices were observed with CLSM from the (i) FITC or (j) rhodamine B channel; Image (k) is the overlap of the two images (the injection sites are indicated by arrows).

xenografted tumors at various doses (Figure 6a–d). Clearly, with the same dose (SN38-eq dose of 10 mg/kg) and dosing schedule, all the micelles showed significantly better tumor growth inhibition activity than irinotecan, the first-line clinically used SN38 derivative anticancer drug, which only slightly slowed down the tumor growth compared with the PBS control (Figure 6a). The tumors treated by the micelles started to regress on day 15 and reached the minimum size on day 37. Unexpectedly, no difference was found in the antitumor efficacies of the two micelles (30 nm *vs* 100 nm) with multi-injection at SN38-eq dose of 10 mg/kg (Figure 6a) or single injection at SN38-eq dose of 30 mg/kg (Figure 6b). The 100 nm micelles showed a significantly better tumor growth inhibition (TGI) than the 30 nm ones (TGI, 44% *vs* 23% on day 27,

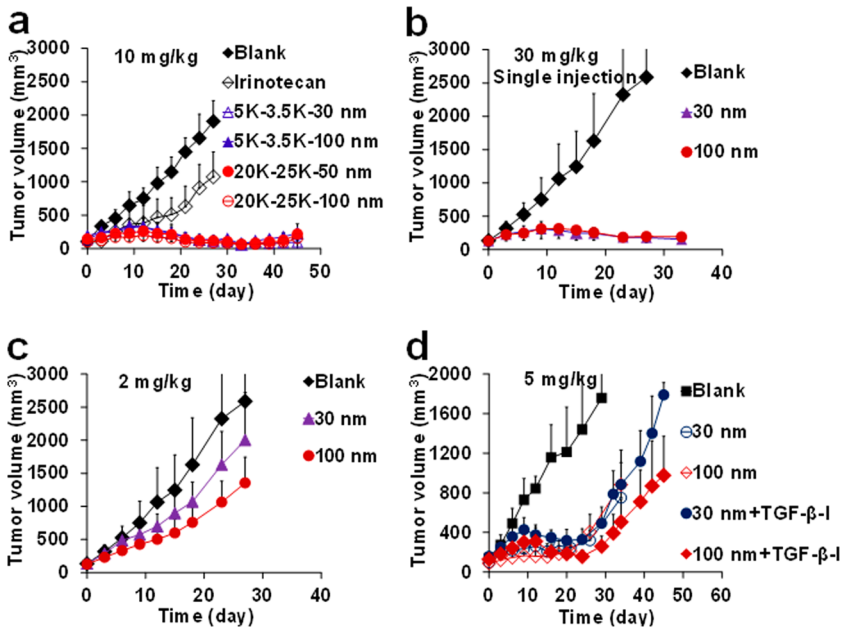

Figure 6. Anticancer activity of micelles tested on BCap37 xenografted tumors. Nude mice bearing xenografted BCap37 tumors of *ca.* 100 mm^3 were used. (a−c) Tumor volume as a function of time of tumor-bearing mice treated with micelles (30 or 100 nm) of PEG_{5K}-$P(HEMASN38)_{3.5K}$ or (50 or 100 nm) of PEG_{20K}-$P(HEMASN38)_{25K}$ at an SN38-eq dose of 10 mg/kg (all q3d × 5) (a), or single intravenous injection of micelles (30 or 100 nm) of PEG_{5K}-$P(HEMASN38)_{3.5K}$ at an SN38-eq dose of 30 mg/kg on day 0 (b), or micelles (30 or 100 nm) of PEG_{5K}-$P(HEMASN38)_{3.5K}$ at an SN38-eq dose of 2 mg/kg (all q3d × 5) (c). (d) TGF-β inhibitor (LY364947) was intraperitoneally injected at a dose of 1 mg/kg (q2d × 7) together with intravenous injection of 30 and 100 nm PEG_{5K}-$P(HEMASN38)_{3.5K}$ micelles at a dose of 5 mg/kg (intravenous, q3d × 5) from day 0. PBS was the negative control, and irinotecan was the positive control. The averaged tumor volume of each group expressed as mean ± SD (n = 6). Bars, SD. Differences in tumor volumes between the treated groups and controlled groups were determined by unpaired student's t-test. The results were considered statistically significant if the two-tailed p-values were less than 0.05. Difference, *$p < 0.05$.

$p < 0.05$) only at substantially reduced dose of 2 mg/kg (Figure 6c). Histological analysis of tumor tissues confirmed the effectiveness of the micelles (10 mg/kg, q3d × 5) in inducing apoptotic death of tumor cells (Figure S11). The tumors in the control and irinotecan-treated groups consisted of tightly packed tumor cells. By contrast, in the micelle-treated groups, the tumor cellularity decreased significantly and was occupied by inflammatory infiltration. This result was consistent with the much higher TGI induced by micelles compared with irinotecan at the same SN38-eq doses.

Co-administration of TGF-β-I can increase the penetration ability of micelles, and thus it was administrated *via* intraperitoneal injection at a dose of 1 mg/kg (q2d × 7), together with intravenous injection of PEG_{5K}-$P(HEMASN38)_{3.5K}$ micelles (30 or 100 nm) at a dose of 5 mg/kg (q3d × 5). An enhanced antitumor activity for 100 nm micelles with TGF-β-I was observed (Figure 6d). The tumors shrank on day 12, which had not been observed for the group with the same treatment but without TGF-β-I (Figure 6d). Furthermore, with the TGF-β-I treatment, the 100 nm micelle-treated group exhibited significantly enhanced antitumor activity than the one treated with 30 nm micelles ($p < 0.05$).

DISCUSSION

Polymeric micelle-based drug delivery systems are generally fabricated from amphiphilic block copolymers with inert hydrophobic blocks, such as PCL and PLA.[30,31] They were limited by low and inconsistent drug loading and unfavorable burst release. Instead, we directly used hydrophobic drugs, such as SN38 or CPT, as the hydrophobic segments of drug delivery carriers to achieve high and fixed drug loading content and avoid burst release.[29,32,33] The amphiphilic prodrug block copolymers based on potent anticancer drug SN38 were synthesized by ATRP of the prodrug monomer, HEMASN38, with PEG-Br as the macroinitiator in DMSO. Considering the difficulty of hydrolyzing the ester of 20-OH in SN38 to release the drug,[32] the methacrylate had to be introduced onto the drug through the phenol (10-OH) in SN38. The formed phenol ester could be cleaved by endogenous thiols, thereby facilitating the prodrug activation in cells,[33] which is critical for polymeric prodrugs. In addition, a linker (succinic acid used here) between SN38 and methacrylate group should be included, otherwise the steric hindrance of the monomer made the polymerization impossible. With the optimization of catalyst type, concentration, and temperature, the amphiphilic SN38 prodrug block copolymers, PEG_x-$P(HEMASN38)_y$, with low polydispersity were successfully synthesized. The PEG contents in the copolymers were set to 40% and 58%, when the copolymer with the hydrophilic block content of these ratios tended to form spherical micelles.[25,26,34]

Other block copolymers have to transform polymer structure to form different sized micelles because an amphiphilic copolymer theoretically can only self-assemble into one thermodynamically stable structure. By contrast, the SN38 prodrug block copolymer surprisingly formed micelles of different sizes through the solvent exclusion method only by tuning the type of solvent, polymer concentration, and the sequence of mixing the polymer solution with water. Their capability of forming different sized micelles resulted from the strong $\pi-\pi$ stacking interaction among the SN38 moieties in the poly(HEMASN38) block, which formed the thermodynamically unstable but dynamically stable structure.[29,33]

The formed micelles, which had the same chemical structures but different sizes, could be an ideal platform to investigate the effects of micelle size on the distribution, blood circulation, tumor accumulation, and penetration of nanoparticulate drugs. Before we used these micelles, we further excluded the effect of possibly varied shape, stability, and charge. These micelles of different sizes were all spherical as observed by TEM and cryo-TEM so that we could exclude the shape effect. Noteworthy, the micelles with bigger sizes, such as 150 and 300 nm, had different internal structures from those with sizes around 100 nm or even smaller ones. The former had an aqueous interior, but the later had a hydrophobic core. Nevertheless, all the micelles were very stable both in the absence and presence of FBS (Figure 1h) with very low critical micellar concentrations (<5 μg/mL; Figures S12 and S13) and had the same slow drug release kinetics, because of the high glass transition temperature (T_g = 125 °C, Figure S14) and the strong $\pi-\pi$ stacking of the SN38 moieties.[29,33]

Moreover, the micelles were all slightly negatively charged, again independent of size and the copolymer structure, and had similar cellular uptake rate and pathway (endocytosis into lysosomes) and thereby same cytotoxicity (Figure 2). Thus, these micelles of different sizes prepared from the same copolymer had similar physical properties except for their size, making them an excellent platform for studying the size effects on the pharmacokinetics, biodistribution, penetration in tumor, and anticancer activity of nanoparticulate drugs. On the other hand, the micelles with the same size (100 nm) but from different block copolymers were also prepared to probe the effects of the block structures.

Considering that the sizes of the micelles were higher than the threshold of kidney clearance (8−10 nm), the liver and spleen were the two main organs responsible for the clearance of micelles from the blood (Figure 4c). The micelles with sizes of around 100 nm had much longer blood circulation time (Figure 3), because they had much lower hepatic uptake than those with smaller sizes of 30 (Figure 4c). For the micelles with similar sizes but different structures, the micelles made from PEG_{2K}-$P(HEMASN38)_{1.4K}$ with short PEG had much shorter blood circulation time than the micelles with 5 kDa or longer PEG chains, because they had much higher liver and splenic accumulation (Figure 4c).

The blood capillaries of subcutaneous tumors are hyperpermeable with pores of cutoff sizes ranging from 200 nm to 1.2 μm, and thus the size (20 to 150 nm) of these micelles might have little effect on their extravasation.[35] Consequently, the tumor accumulation of the micelles at 24 h was shown to be mainly determined by their blood circulation times (p < 0.001, Correlation Coefficient = 0.988) and bioavailabilities (AUCs) (p < 0.001, Correlation Coefficient = 0.988) instead of size (p > 0.5, Correlation Coefficient = 0.541). Micelles with short blood circulation had low tumor drug concentration quickly leveling off over time, whereas those with long blood circulation had much higher drug accumulation in tumor, which gradually increased over time because of their higher blood drug concentrations during the period (Figure 5a). At 24 h postinjection, consistent with the 10-fold higher AUC of the 100 nm micelles than that of 35 nm micelles from PEG_{5K}-$P(HEMASN38)_{3.5K}$, the tumor drug concentration of 100 nm micelles reached 12% ID/g, about 10 times that for the 35 nm micelles. The 100 nm micelle from PEG_{20K}-$P(HEMASN38)_{25K}$ even achieved 20% ID/g tumor tissue, about 20 times of that for the 35 nm PEG_{5K}-$P(HEMASN38)_{3.5K}$ micelles at 24 h postinjection.

The micelles showed the expected higher therapeutic efficacy than the first-line clinically used irinotecan[33] probably because of their improved pharmacokinetics and diverse intracellular behaviors. However, very unexpectedly, the high tumor accumulation of the 100 nm micelle did not lead to high therapeutic efficacy. The five intravenous treatments at SN38-eq doses of 5 and 10 mg/kg or a single intravenous treatment at 30 mg/kg, the 30 and 100 nm micelles showed no difference in therapeutic efficacies even though the 100 nm micelles accumulated 10 times more in tumor than the 30 nm micelles. Given that these micelles had similar cellular uptakes (Figure 2d and 2e), drug releases (Figure S7), and even cytotoxicities (Figure 2f, g), the inability to produce high therapeutic efficacy of the high drug concentration for the 100 nm micelles was probably due to their limited diffusion and thus reduced availability to the tumor cells because of their large size. This result was validated by observing the micelle distribution in the tumor using CLSM. The 30 nm fluorescence-labeled micelles had low intensity in the tumor, but they were distributed in the whole tumor. By contrast, the fluorescent 100 nm micelles had much higher intensity in the tumor, but they were restricted in the vicinity of blood vessels (Figure 5c−d). The administration of TGF-β-I was shown to be able to improve the penetration of 100 nm micelles (Figure 5e).

The difference in diffusivity of the two different sized micelles was more clearly distinguished by the intratumoral injection experiment. Under similar experimental conditions, the 30 nm micelles diffused much farther away from the injection site compared with the 100 nm micelles (Figure 5i–k). Thus, the little improvement in the therapeutic efficacy for the 100 nm micelles over the 30 nm micelles was probably due to the fact that their higher accumulation in tumor was canceled out by their worse tumor penetration capability.

To further confirm this conclusion, along with the intravenous treatment with the micelles at a dose of 5 mg/kg (q3d × 5), TGF-β inhibitor was administered intraperitoneally (q2d × 7) to relax the tumor extracellular matrix and thus increase the penetration of large micelles. This treatment significantly enhanced the antitumor activity of the 100 nm micelles but had little effects on the 30 nm ones (Figure 6d).

CONCLUSION

From the well-defined drug conjugated block copolymer PEG_x-P(HEMASN38)$_y$, a series of micelles with different sizes were fabricated and used to investigate the size-dependence of blood clearance, tumor accumulation and penetration, and anticancer activity. We demonstrated that micelle size strongly affected blood clearance rate, and the size-dependence differed at micelle size of approximately 100 nm. The blood clearance became slower as the micelle size increased up to around 100 nm. The micelles in the range of 100 to 160 nm had very similar blood clearance rates. Further increase in micelle size hastened their blood clearance. Small micelles (*e.g.*, 35 nm) were mainly cleared by the liver, whereas large micelles (*e.g.*, 150 nm) were mainly sequestered by the spleen in terms of drug concentration in organs. The tumor accumulation of the micelles was directly proportional to their blood circulation time. After intravenous administration, the long circulating 100 nm micelles could accumulate 10 to 20 times more in BCap37 xenografted tumors than the 30 nm micelles. However, the higher tumor drug concentration did not lead to higher anticancer activity, probably because the 100 nm micelles had lower penetration in tumors than the 30 nm micelles. Thus, the future design of nanoparticulate drug for high anticancer efficacy should always balance the size for accumulation and penetration; *i.e.*, the particle should be large enough for long circulation and tumor accumulation but small enough for good tumor penetration.

METHODS

Materials, Cell Lines, and Animals. The descriptions of the materials, cell lines (Bcap 37 cell lines) and animals are provided in the Supporting Information. All animal studies were approved by the Animal Care and Use Committee of Zhejiang University in accordance with the Chinese guidelines for the care and use of laboratory animals.

Syntheses of Polymeric Prodrugs. PEGx-P(HEMASN38)y of different block lengths were prepared *via* ATRP, and the detailed procedures are described in the Supporting Information. Rhodamine B and FITC labeled PEGx-P(HEMASN38)y were prepared *via* the reaction of PEGx-P(HEMASN38)y with the product of the reaction between cysteamine and rhodamine B isocyanate or FITC. The detailed synthesis procedures are given in the Supporting Information.

Preparation and Characterization of Polymeric Prodrug Micelles. Polymeric prodrug micelles of different sizes were prepared by adding PEGx-P(HEMASN38)y DMSO or DMF solutions at different concentrations into DI water of double volume under stirring or reversely. The size, size distribution and ζ-potential were determined using a Zetasizer Nano-ZS (Malvern Instruments, UK). The morphologies of polymeric prodrug micelles were observed by TEM or Cryogenic TEM. The detailed information on the preparation and characterization is given in the Supporting Information.

***In Vitro* Assays.** The SN 38 release behavior, critical micelle concentration (CMC), cytotoxicity, cellular uptake, subcellular distribution of polymer prodrug micelles were tested according to the procedure described in the Supporting Information.

Blood Clearance Measurement. Female ICR mice (~25 g) were used. Prodrugs (SN38-eq dose of 5 mg/kg) were i.v. administrated *via* tail vein. At timed intervals, 50 μL blood samples were collected into microtubes containing 50 μL 0.1 N NaOH solution, and incubated at 45 °C for 24 h. Then the samples were precipitated by adding 1 mL acetonitrile. After centrifugation, 200 μL supernate was acidized by 200 μL 0.1 N HCl aqueous solution before HPLC analysis.

Biodistribution Measurement. Nude mice bearing xenografted Bcap37 tumors of *ca.* 100 mm^3 were i.v. injected with micelles (SN38-eq dose of 5 mg/kg). At timed intervals, the nude mice were sacrificed and organs were collected. The organs were added to 2-fold weight of water and homogenized. The homogenized organs were first treated by equal volume of 0.1 N NaOH for 24 h at 37 °C and subsequently precipitated by adding 10-fold volume of acetonitrile. After centrifugation, 200 μL of the supernate was acidized by the same volume of 0.1 N HCl solution. The SN38 concentration in the samples was determined by HPLC.

The extraction efficiency of SN38 from organs was determined by adding known amount of micelles to organs of predetermined weights, and the mixture were treated with the same method mentioned above. The theoretical SN38 concentration was set to 100%.

***In Vivo* Antitumor Activity Assay.** BALB/c nude mice (aged 6–8 weeks) were inoculated subcutaneously with Bcap37 cells (1×10^6 cells suspended in 0.2 mL of PBS). When the tumor volume reached ~100 mm^3, mice were randomly divided into test groups. Treatments were carried out on day 0, 3, 6, 9, and 12 by i.v. injection *via* the tail vein. The experiment was operated on several different SN38-eq doses: 10 mg/kg (q3d × 5), 5 mg/kg (q3d × 5), 2 mg/kg (q3d × 5), or a single injection of 30 mg/kg. A coadministration of i.v. injection of micelles at SN38-eq dose of 5 mg/kg (q3d × 5) with intraperitoneally injection of 1 mg/kg of TGF-β-I (q2d × 7) were also performed in two groups.

Antitumor activity was evaluated in terms of tumor volume (TV), which was estimated as follows: $TV = a \times b^2/2$, where a and b are the major and minor axes of tumors, respectively, as measured by a caliper.

Microdistribution of Fluorescently Labeled Micelles in Tumors or Organs. Nude mice bearing xenografted BCap37 tumors (~200 mm^3) were i.v. injected with Rhodamine B labeled 30 or 100 nm PEG_{5K}-P(HEMASN38)$_{3.5K}$ micelles. All mice were injected with FITC labeled *Lycopersicon esculentum* lectin 5 min before sacrifice to indicate blood vessels (green). The tumor tissues at 24 h were respectively excised and sectioned (thickness, 10 μm) in a

cryostat and observed by CLSM (Nikon, A1). The histological analyses of micelles in liver and spleens were determined in the same way.

Microdistribution of Fluorescently Labeled Micelles in Tumors after Intratumor Injections. Nude mice bearing BCap37 xenografted tumors (~100 mm^3) were intratumor injected with mixed aqueous solution containing 30 nm (FITC labeled) and 100 nm (Rhodamine B labeled) micelles. The fluorescence intensities of 30 and 100 nm micelles were adjusted to be the same. Tumors were collected after 72 h and immediately frozen and further sectioned (thickness, 10 μm) in a cryostat. The tumor sections were observed with the same excited power of laser on a CLSM (Nikon, A1).

Enhancement of Tumor Permeability by Treatment with a TGF-β Inhibitor. Nude mice bearing BCap37 xenografted tumors (~100 mm^3) were intraperitoneally administered TGF-β inhibitor LY364947 at 1 mg/kg at 1h before i.v. injection of 100 nm Rhodamine B labeled micelles. Tumors were collected after 24 h and observed as described above.

Histological Examination of Tumor Tissues. The xenografted tumors were excised and fixed in 4% neutral buffered paraformaldehyde before embedded in paraffin to make tissue sections. Tissue sections of 10 μm thickness were prepared and stained with hematoxylin and esion (H&E, Fisher Scientific, USA) for histological examinations. The histological identification of apoptotic cells has been described and illustrated in previous publications.[33]

Statistical Analyses. The pharmacokinetic parameters, including half-life time ($t_{0.5\beta}$) and areas under curve (AUC) were estimated by fitting the SN38 concentration in plasma into a two-compartment model (Loo-Riegelman method) by the nonlinear least-squares method using 3P87 software. The correlations between tumor accumulations of micelles at 24 h postinjection and sizes, half-life times ($t_{0.5\beta}$s) or bioavailabilities (AUCs) were determined using two-tailed person's analysis with SPSS statistical software. Differences in tumor volume between the treated groups and controlled groups were determined by unpaired student's *t*-test. The results were considered statistically significant if the two-tailed P-values were less than 0.05.

Conflict of Interest: The authors declare no competing financial interest.

Acknowledgment. This work was financially supported by the National Nature Science Foundation of China (51390481, 21174128 and 21274125), National Basic Research Program. Grant Number: 2014CB931900 and the Specialized Research Fund for the Doctoral Program of Higher Education of China (Grant No. 20110101130007).

Supporting Information Available: The detailed synthesis procedures, preparation, characterization and *in vitro* assays of the polymer prodrug micelles plus the supplementary data. The Supporting Information is available free of charge on the ACS Publications website at DOI: 10.1021/acsnano.5b02017.

REFERENCES AND NOTES

1. Duncan, R.; Vicent, M. J. Polymer Therapeutics-Prospects for 21st Century: The End of the Beginning. *Adv. Drug Delivery Rev.* **2013**, *65*, 60–70.
2. Lee, J. L.; Ahn, J. H.; Park, S. H.; Lim, H. Y.; Kwon, J. H.; Ahn, S.; Song, C.; Hong, J. H.; Kim, C. S.; Ahn, H. Phase II Study of a Cremophor-Free, Polymeric Micelle Formulation of Paclitaxel for Patients with Advanced Urothelial Cancer Previously Treated with Gemcitabine and Platinum. *Invest. New Drugs* **2012**, *30*, 1984–1990.
3. Lee, K. S.; Chung, H. C.; Im, S. A.; Park, Y. H.; Kim, C. S.; Kim, S. B.; Rha, S. Y.; Lee, M. Y.; Ro, J. Multicenter Phase II Trial of Genexol-PM, a Cremophor-Free, Polymeric Micelle Formulation of Paclitaxel, in Patients with Metastatic Breast Cancer. *Breast Cancer Res. Treat.* **2008**, *108*, 241–250.
4. Lammers, T.; Kiessling, F.; Hennink, W. E.; Storm, G. Drug Targeting to Tumors: Principles, Pitfalls and (pre-) Clinical Progress. *J. Controlled Release* **2012**, *161*, 175–187.
5. Ming, C.; Xiangrui, L.; Jianbin, T.; Meihua, S.; Youqing, S. Facile Synthesis of Size-Tunable Stable Nanoparticles *via* Click Reaction for Cancer Drug Delivery. *Sci. China: Chem.* **2014**, *57*, 633–644.
6. Shiyong, Z.; Yao, W.; Bin, H.; Kui, L.; Zhongwei, G. Biodegradable Polymeric Nanoparticles Based on Amphiphilic Principle: Construction and Application in Drug Delivery. *Sci. China: Chem.* **2014**, *57*, 461–475.
7. Maeda, H.; Wu, J.; Sawa, T.; Matsumura, Y.; Hori, K. Tumor Vascular Permeability and the EPR Effect in Macromolecular Therapeutics: A Review. *J. Controlled Release* **2000**, *65*, 271–284.
8. Davis, M. E.; Chen, Z.; Shin, D. M. Nanoparticle Therapeutics: An Emerging Treatment Modality for Cancer. *Nat. Rev. Drug Discovery* **2008**, *7*, 771–782.
9. Stirland, D. L.; Nichols, J. W.; Miura, S.; Bae, Y. H. Mind the gap: A Survey of How Cancer Drug Carriers Are Susceptible to the Gap Between Research and Practice. *J. Controlled Release* **2013**, *172*, 1045–1064.
10. Barenholz, Y. Doxil (R) - The First FDA-Approved Nano-Drug: Lessons Learned. *J. Controlled Release* **2012**, *160*, 117–134.
11. Sun, Q. H.; Sun, X. R.; Ma, X. P.; Zhou, Z. X.; Jin, E. L.; Zhang, B.; Shen, Y. Q.; Van Kirk, E. A.; Murdoch, W. J.; Lott, J. R.; *et al.* Integration of Nanoassembly Functions for an Effective Delivery Cascade for Cancer Drugs. *Adv. Mater. (Weinheim, Ger.)* **2014**, *26*, 7615–7621.
12. Kanapathipillai, M.; Brock, A.; Ingber, D. E. Nanoparticle targeting of anti-cancer drugs that alter intracellular signaling or influence the tumor microenvironment. *Adv. Drug Delivery Rev.* **2014**, *79—80*, 107–118.
13. Khawar, I. A.; Kim, J. H.; Kuh, H. J. Improving drug delivery to solid tumors: Priming the tumor microenvironment. *J. Controlled Release* **2015**, *201*, 78–89.
14. Ozcelikkale, A.; Ghosh, S.; Han, B. Multifaceted Transport Characteristics of Nanomedicine: Needs for Characterization in Dynamic Environment. *Mol. Pharmaceutics* **2013**, *10*, 2111–2126.
15. Alexis, F.; Pridgen, E.; Molnar, L. K.; Farokhzad, O. C. Factors Affecting the Clearance and Biodistribution of Polymeric Nanoparticles. *Mol. Pharmaceutics* **2008**, *5*, 505–515.
16. Moghimi, S. M.; Hunter, A. C.; Andresen, T. L. Factors Controlling Nanoparticle Pharmacokinetics: An Integrated Analysis and Perspective. *Annu. Rev. Pharmacol. Toxicol.* **2012**, *52*, 481–503.
17. Attia, A. B. E.; Yang, C.; Tan, J. P. K.; Gao, S. J.; Williams, D. F.; Hedrick, J. L.; Yang, Y. Y. The Effect of Kinetic Stability on Biodistribution and Anti-Tumor Efficacy of Drug-Loaded Biodegradable Polymeric Micelles. *Biomaterials* **2013**, *34*, 3132–3140.
18. Perrault, S. D.; Walkey, C.; Jennings, T.; Fischer, H. C.; Chan, W. C. W. Mediating Tumor Targeting Efficiency of Nanoparticles Through Design. *Nano Lett.* **2009**, *9*, 1909–1915.
19. Gratton, S. E. A.; Ropp, P. A.; Pohlhaus, P. D.; Luft, J. C.; Madden, V. J.; Napier, M. E.; DeSimone, J. M. The Effect of Particle Design on Cellular Internalization Pathways. *Proc. Natl. Acad. Sci. U. S. A.* **2008**, *105*, 11613–11618.
20. Christian, D. A.; Cai, S. S.; Garbuzenko, O. B.; Harada, T.; Zajac, A. L.; Minko, T.; Discher, D. E. Flexible Filaments for *in Vivo* Imaging and Delivery: Persistent Circulation of Filomicelles Opens the Dosage Window for Sustained Tumor Shrinkage. *Mol. Pharmaceutics* **2009**, *6*, 1343–1352.
21. Geng, Y.; Dalhaimer, P.; Cai, S. S.; Tsai, R.; Tewari, M.; Minko, T.; Discher, D. E. Shape Effects of Filaments *Versus* Spherical Particles in Flow and Drug Delivery. *Nat. Nanotechnol.* **2007**, *2*, 249–255.
22. Huang, K. Y.; Ma, H. L.; Liu, J.; Huo, S. D.; Kumar, A.; Wei, T.; Zhang, X.; Jin, S. B.; Gan, Y. L.; Wang, P. C.; *et al.* Size-Dependent Localization and Penetration of Ultrasmall Gold Nanoparticles in Cancer Cells, Multicellular Spheroids, and Tumors *in Vivo*. *ACS Nano* **2012**, *6*, 4483–4493.
23. Lee, H.; Fonge, H.; Hoang, B.; Reilly, R. M.; Allen, C. The Effects of Particle Size and Molecular Targeting on the Intratumoral and Subcellular Distribution of Polymeric Nanoparticles. *Mol. Pharmaceutics* **2010**, *7*, 1195–1208.

24. Cabral, H.; Matsumoto, Y.; Mizuno, K.; Chen, Q.; Murakami, M.; Kimura, M.; Terada, Y.; Kano, M. R.; Miyazono, K.; Uesaka, M.; *et al.* Accumulation of sub-100 nm Polymeric Micelles in Poorly Permeable Tumours Depends on Size. *Nat. Nanotechnol.* **2011**, *6*, 815–823.
25. Schadlich, A.; Caysa, H.; Mueller, T.; Tenambergen, F.; Rose, C.; Gopferich, A.; Kuntsche, J.; Mader, K. Tumor Accumulation of NIR Fluorescent PEG PLA Nanoparticles: Impact of Particle Size and Human Xenograft Tumor Model. *ACS Nano* **2011**, *5*, 8710–8720.
26. Gref, R.; Luck, M.; Quellec, P.; Marchand, M.; Dellacherie, E.; Harnisch, S.; Blunk, T.; Muller, R. H. 'Stealth' Corona-Core Nanoparticles Surface Modified by Polyethylene Glycol (PEG): Influences of the Corona (PEG Chain Length and Surface Density) and of the Core Composition on Phagocytic Uptake and Plasma Protein Adsorption. *Colloids Surf., B* **2000**, *18*, 301–313.
27. Tyrrell, Z. L.; Shen, Y.; Radosz, M. Fabrication of Micellar Nanoparticles for Drug Delivery Through the Self-Assembly of Block Copolymers. *Prog. Polym. Sci.* **2010**, *35*, 1128–1143.
28. Minowa, T.; Kawano, K.; Kuribayashi, H.; Shiraishi, K.; Sugino, T.; Hattori, Y.; Yokoyama, M.; Maitani, Y. Increase in Tumour Permeability Following TGF-beta Type I Receptor-Inhibitor Treatment Observed by Dynamic Contrast-Enhanced MRI. *Br. J. Cancer* **2009**, *101*, 1884–1890.
29. Shen, Y. Q.; Jin, E. L.; Zhang, B.; Murphy, C. J.; Sui, M. H.; Zhao, J.; Wang, J. Q.; Tang, J. B.; Fan, M. H.; Van Kirk, E.; *et al.* Prodrugs Forming High Drug Loading Multifunctional Nanocapsules for Intracellular Cancer Drug Delivery. *J. Am. Chem. Soc.* **2010**, *132*, 4259–4265.
30. Jin, E.; Zhang, B.; Sun, X.; Zhou, Z.; Ma, X.; Sun, Q.; Tang, J.; Shen, Y.; Van Kirk, E.; Murdoch, W. J.; *et al.* Acid-Active Cell-Penetrating Peptides for *in Vivo* Tumor-Targeted Drug Delivery. *J. Am. Chem. Soc.* **2012**, *135*, 933–940.
31. Wu, X.; Sun, X.; Guo, Z.; Tang, J.; Shen, Y.; James, T. D.; Tian, H.; Zhu, W. *In Vivo* and in Situ Tracking Cancer Chemotherapy by Highly Photostable NIR Fluorescent Theranostic Prodrug. *J. Am. Chem. Soc.* **2014**, *136*, 3579–3588.
32. Zhang, H. F.; Wang, J. Q.; Mao, W. W.; Huang, J.; Wu, X. G.; Shen, Y. Q.; Sui, M. H. Novel SN38 Conjugate-Forming Nanoparticles as Anticancer Prodrug: *In Vitro* and *in Vivo* Studies. *J. Controlled Release* **2013**, *166*, 147–158.
33. Wang, J. R.; Sun, X. R.; Mao, W. W.; Sun, W. L.; Tang, J. B.; Sui, M. H.; Shen, Y. Q.; Gu, Z. W. Tumor Redox Heterogeneity-Responsive Prodrug Nanocapsules for Cancer Chemotherapy. *Adv. Mater. (Weinheim, Ger.)* **2013**, *25*, 3670–3676.
34. Avgoustakis, K.; Beletsi, A.; Panagi, Z.; Klepetsanis, P.; Livaniou, E.; Evangelatos, G.; Ithakissios, D. S. Effect of Copolymer Composition on the Physicochemical Characteristics, *in Vitro* Stability, and Biodistribution of PLGA-mPEG Nanoparticles. *Int. J. Pharm. (Amsterdam, Neth.)* **2003**, *259*, 115–127.
35. Hobbs, S. K.; Monsky, W. L.; Yuan, F.; Roberts, W. G.; Griffith, L.; Torchilin, V. P.; Jain, R. K. Regulation of Transport Pathways in Tumor Vessels: Role of Tumor Type and Microenvironment. *Proc. Natl. Acad. Sci. U. S. A.* **1998**, *95*, 4607–4612.